

Search for serendipitous TNO occultation in X-rays

Hsiang-Kuang Chang^{1,2*}, Chih-Yuan Liu^{2,3}, and Kuan-Ting Chen²

¹*Institute of Astronomy, National Tsing Hua University, Hsinchu 30013, Taiwan*

²*Department of Physics, National Tsing Hua University, Hsinchu 30013, Taiwan*

³*LESIA, Paris Observatory, 92195 Meudon, France*

Accepted November 19, 2012

ABSTRACT

To study the population properties of small, remote objects beyond Neptune’s orbit in the outer solar system, of kilometer size or smaller, serendipitous occultation search is so far the only way. For hectometer-sized Trans-Neptunian Objects (TNOs), optical shadows actually disappear because of diffraction. Observations at shorter wave lengths are needed. Here we report the effort of TNO occultation search in X-rays using RXTE/PCA data of Sco X-1 taken from June 2007 to October 2011. No definite TNO occultation events were found in the 334 ks data. We investigate the detection efficiency dependence on the TNO size to better define the sensible size range of our approach and suggest upper limits to the TNO size distribution in the size range from 30 m to 300 m. A list of X-ray sources suitable for future larger facilities to observe is proposed.

Key words: occultations – Kuiper Belt – Solar system: formation – stars: neutron – X-rays: binaries.

1 INTRODUCTION

Serendipitous Trans-Neptunian Object (TNO) occultation search is so far the only way to explore properties of kilometer-sized TNOs or smaller. Such search has been being conducted mainly in optical bands (Bianco et al. 2010; Bickerton, Kavelaars & Welch 2008; Roques et al. 2003) with few reported detections (Roques et al. 2006; Schlichting et al. 2009, 2012). In the X-ray band, occultation by smaller objects may be detected because of a smaller Fresnel scale. Following an earlier discovery of putative occultation events, allegedly caused by 100-meter size TNOs, in the 1996-2002 X-ray data of Sco X-1 taken by the instrument Proportional Counter Array (PCA) on board Rossi X-ray Timing Explorer (RXTE) (Chang et al. 2006, 2007), we conducted new RXTE/PCA observations of Sco X-1 from June 2007 to Oct 2011 to clarify possible instrumental-effect contamination in that discovery.

In this paper we report the final result of the effort in the search for serendipitous TNO occultation in X-rays with RXTE/PCA, taking into account the issue of detection efficiency. Earlier results based on data taken by Oct 2009 have been published in Liu et al. (2008) and Chang et al. (2011). Currently such search is only feasible with RXTE/PCA observation of Sco X-1, because of the large effective area of PCA and because Sco X-1 is the brightest X-ray source in the sky (Chang et al. 2006, 2007). Since RXTE was decom-

missioned in January 2012, new efforts have to await possible larger instruments in the future.

TNOs larger than deca-kilometer size can be detected directly. Results of those observations can be found in Fuentes et al. (2010) and Fuentes, Trilling & Holman (2011) for works using HST, in Fraser, Brown & Schwamb (2010) for Subaru, and in Petit et al. (2011) for CFHT. The TNO size distribution, from thousand-kilometer to decameter size and smaller, carries information of the collisional and dynamical history of the early solar system. It is of essential importance to our understanding of how the solar system formed (see e.g. Chiang et al. (2007), Benavidez & Bagatin (2009), Fraser (2009) and Kenyon & Bromley (2012)).

2 SUMMARY OF THE RXTE/PCA 2007-2011 OBSERVATIONS

RXTE had observed Sco X-1 for many times, and yielded a large amount of data by 2007 (for details of RXTE instruments, see Jahoda et al. (2006)). Many millisecond-dip events were found in those data (Chang et al. 2006), but later it was pointed out that ‘Very Large Events’ (VLEs) are likely the cause of those dips, rather than TNO occultations (Chang et al. 2007; Jones et al. 2008). VLEs are events that deposit more than 100 keV into an individual anode in a Proportional Counter Unit (PCU). RXTE/PCA consists of 5 identical PCUs. An instrument dead-time of 50 μ s is set for each VLE during RXTE observations of Sco X-1. VLEs

* E-mail: hkchang@phys.nthu.edu.tw

Type	number of triggered anodes	average count rate
A	no	1.73 ± 0.29
B	all	34.5 ± 11.0
C	more than one but not all	44.7 ± 9.97
D	only one	9.37 ± 2.17

Table 1. VLE types and their average count rates (in units of counts per second per PCU). The number of PCUs which are on during the observation varies from time to time. The total data employed in this analysis is 334 ksec, and is 1363 ksec-PCU when the number of PCU on is taken into account.

Group	associated VLE type	significant dips	less significant dips
A	Type A	45	180
B	Type B, no Type A	2	142
C	Type C, no Type A, B	3	35
D	Type D only	0	6
E	no VLEs	1	10

Table 2. Number of dips in different groups. ‘Significant’ dips are those with the number of counts smaller than -6.5σ below the average in an 8-second running window, where σ is the standard deviation of the counts in each bin in the running window. ‘Less significant’ dips are those below -5.0σ but higher than -6.5σ .

are produced by high-energy photons or particles. Whether they are really the cause of the millisecond dip events found earlier, however, was not conclusive because VLEs were only recorded in housekeeping data with a coarse time resolution of 125 ms in the data taken by 2007. In order to clarify the possible instrumental effect that may have caused the millisecond dip events found in Chang et al. (2006, 2007), new observations with a newly designed data mode to record more detailed information of each individual VLE, such as the identification of the triggered PCU and the triggered anode and timing with 125 μ s accuracy, were conducted from June 2007 to October 2011, which produced in total 334 ks data good for the search for serendipitous TNO occultations.

As already reported in Chang et al. (2011), if one distinguishes VLEs into different types according to the number of anodes that were triggered, one can find that indeed millisecond dip events are associated with VLEs of different types in a systematic manner. The average count rate for all VLEs altogether in the 334-ks data is 90.3 ± 18.8 counts per second per PCU. The rate for each type of VLEs is shown in Table 1. To see the association of dip events with VLEs, we divide dip events into groups according to their associated VLE types, as shown in Table 2. For more detailed description of these classifications, as well as the algorithm that we used to find and define the dip event, see Chang et al. (2011).

From Table 2 we can see that 45 of the 51 significant dips are of Group A. Type-A VLE only has a count rate of 1.73 ± 0.29 counts per second per PCU. Apparently Type-A VLEs are very strong events that cause these dips, although exact details and why they are recorded with no anode triggered are not yet understood. The issue whether Type-B, -C, and -D VLEs can also produce millisecond dips

was discussed in Chang et al. (2011) based on the number of ‘less significant’ dips. In our search algorithm, we in fact rounded off the value of count deviations to the first decimal, so all those dips with deviation between -4.95σ and -6.45σ were counted as ‘less significant’ dips. Since most of the dips are of 2-ms duration, we consider only the case of 2-ms bins (more precisely speaking, each 2-ms bin in fact is $8/4096$ s = 1.95 ms). There are 1.71×10^8 ‘2-ms’ bins in total in the 334-ks data. The expected number of ‘less significant’ dips due to random fluctuation is 63.4 if a Gaussian distribution is assumed. The deviation distribution of the data is a dead-time-corrected Poisson distribution, which is about a factor of $2 \sim 3$ smaller than a Gaussian at about -5σ ; see the discussion and Figure 1 in Chang et al. (2011). We therefore consider the total number of less significant dips to be $63.4/2.5 = 25.4$. Among the 1.71×10^8 bins, 9.1×10^7 bins are without the occurrence of any VLEs. The number of these 25.4 dips in Group E can be estimated to be $25.4 \times 9.1/17.1 = 13.5$. That of the other groups can be estimated with the corresponding VLE count rates. We therefore expect the numbers of ‘less significant’ dips to be 0.23, 4.54, 5.88, 1.23, and 13.5 for Group A to E respectively. From Table 2 one can see that only that of Group E is consistent with random fluctuation. The numbers of ‘less significant’ dips of other groups are clearly larger. The deviation is the largest for Group A, and gets smaller and smaller from Group A to D. The above estimate is only a rough one because (1) we consider only the case of 2-ms bins, i.e. treating all the dips as of duration 2 ms, (2) in our definition of dip groups, Type B VLEs can also occur in Group A dips, similarly for Type C and D VLEs, so the use of each VLE count rates for the estimation is not an accurate one, and (3) the factor 2.5 to account for the difference from a Gaussian distribution is somewhat arbitrary. Nonetheless, we think the above estimate is good enough to indicate the VLE-association of those dips in Group A to D.

Those significant dips are not due to random fluctuation. The above discussion strongly suggests that those of Group A to D are related to the occurrence of VLEs and are therefore instrumental due to a process not yet fully understood. The ‘significant’ dip event in Group E, denoted as ‘Event E1’ in Chang et al. (2011), is the only non-random dip event that shows no indication of any instrumental effect. Its light curve was fit with shadow diffraction patterns in Chang et al. (2011) and the result suggests that it is probably not due to TNO occultation either.

In this section we update the results presented in Chang et al. (2011) and have the same conclusion: (1) The fact that most of the ‘significant’ dip events are in Group A indicates that Group-A dips are instrumental. (2) The numbers of ‘less significant’ dip events of Group A, B, C and D are larger than expected from random fluctuation. It strongly suggests that VLEs, even for Type D, which triggers only one anode, can result in millisecond dip events. Only those dips without any association with VLEs can be considered non-instrumental.

3 THE DETECTION EFFICIENCY

In our earlier study to infer the TNO size distribution, a 100% detection efficiency was assumed. To better under-

stand the detection efficiency of our approach, we conducted simulations to investigate the dependence of detection efficiency on the size and relative transverse speed of the occulting body. The detection efficiency surely also depends on the observed count rate, which is related to the brightness of the occulted background source and the instrument employed. In the following we consider two different count rates. One is 8×10^4 cps, which is close to what we usually have for RXTE/PCA observations of Sco X-1. The other is 2×10^6 cps, which is about 20 times more than RXTE/PCA and could be achieved by future missions such as the proposed LOFT project (Mignani et al. 2011). The orbital speed of the Earth is about 30 km/s. That at 40 AU is 5 km/s. The orbital speed of the RXTE spacecraft relative to the Earth is 7.8 km/s. Sco X-1 is in a direction at about 5.5° to the north of the ecliptic. The relative transverse (to the line of sight) speed of an occulting body is usually largest when Sco X-1 is in opposition (around end May) and smallest when the Earth moves towards or away from the direction of Sco X-1. The orientation of the motion of RXTE and of the occulting body will also affect that speed. We therefore consider three different speeds, i.e. 5, 15 and 25 km/s, in the simulation respectively.

For a given count rate and a given transverse speed, we would like to know the chance of detecting an occultation event caused by an occulting body of a certain size with our searching algorithm. Most of the RXTE/PCA-observed photons from Sco X-1 are about 4 keV in energy (0.3 nm in wavelength). The Fresnel scale, which is defined as $\sqrt{\lambda d/2}$, where λ is the wavelength and d the distance, is 30 m for $\lambda = 0.3$ nm and $d = 40$ AU. One expects to detect the shadow of an occulting body much larger than the Fresnel scale easily, while that of a body much smaller than the Fresnel scale will elude being detected due to diffraction. Another factor significantly affecting the observed shadow (light curve) is the impact parameter β , usually defined to be the shortest distance of the passing path to the shadow center in units of the occulting body radius. A few shadow diffraction patterns, computed with the recipes in Roques, Moncuquet & Sicardy (1987) and with a typical RXTE/PCA-observed Sco X-1 photon spectrum, are shown in Figure 1. We note that with a point background source the diffraction patterns, expressed in units of the Fresnel scale, are all the same for a fixed ratio of the occulting body size to the Fresnel scale. That is, there is a size-distance degeneracy. Attempts to break this degeneracy are discussed in the next section. We adopt the definition of the shadow boundary employed in Nihei et al. (2007), in which the relation between the shadow size Ω and the occulting body radius ρ is described as $\Omega = 2(\sqrt{3}^{3/2} + \rho^{3/2})^{2/3}$, in which both Ω and ρ are in units of a Fresnel scale. Throughout this paper, when referring to the occulting body size we will use the diameter D , which is obviously equal to 2ρ .

In our simulation, with a given count rate F , a given transverse speed v , and a given occulting body diameter D , we randomly pick an impact parameter β in the range from the shadow center ($\beta = 0$) to its boundary ($\beta = \frac{\Omega}{2}$) with a uniform probability and a random epoch for each individual implanted event in a 100-s segment. We first compute such a 100-s model light curve, then bin the light curve into 0.25-ms bins, and then randomize the counts in each bin

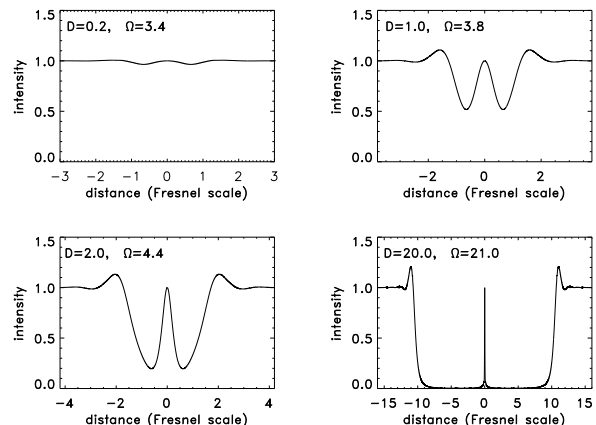


Figure 1. Computed shadow light curves for occulting bodies of different diameter D . All the 4 panels are for the case of a central-crossing event, that is, for a zero impact parameter β . A typical RXTE/PCA observed Sco X-1 spectrum is used for the diffraction pattern computation. Ω is the shadow width as defined in Nihei et al. (2007). D and Ω are both in units of a Fresnel scale.

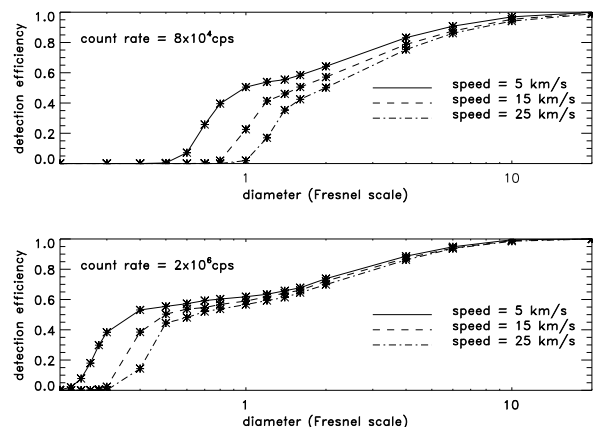


Figure 2. The detection efficiency of our algorithm in the search for serendipitous TNO occultations as a function of the occulting body diameter. Three different relative transverse speeds are considered. We assume these occulting bodies are at 40 AU away, that is, one Fresnel scale corresponds to 30 m. The upper panel is for the case of the typical RXTE/PCA count rate, and the lower one is for a much higher count rate, which may be achieved by future missions.

to produce a simulated binned light curve. This light curve is then processed with exactly the same algorithm that we apply to real data. We repeat the procedure 10^5 times for each set of F , v and D , and record the number of times of detection, which we use to represent the detection efficiency.

The result of the detection efficiency determination is shown in Figure 2. One can see that, with the current RXTE/PCA count rate, a detection efficiency larger than 50% can be achieved for occulting bodies larger than 2 Fresnel scale (diameter), considering the case of relative transverse speed being 25 km/s, while for the high count rate case (2×10^6 cps), that occulting body size can be pushed down to about 0.6 Fresnel scale.

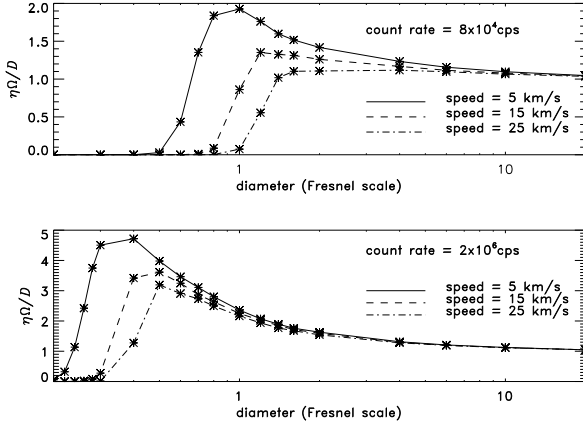


Figure 3. The difference between the detection efficiency times shadow width ($\eta\Omega$) and the occulting body diameter (D) expressed in the form of their ratio as a function occulting body diameter. For larger occulting bodies the fractional difference is small. For smaller ones whose detection efficiency is not yet negligible it becomes large since the shadow width approaches a constant value when the size decreases.

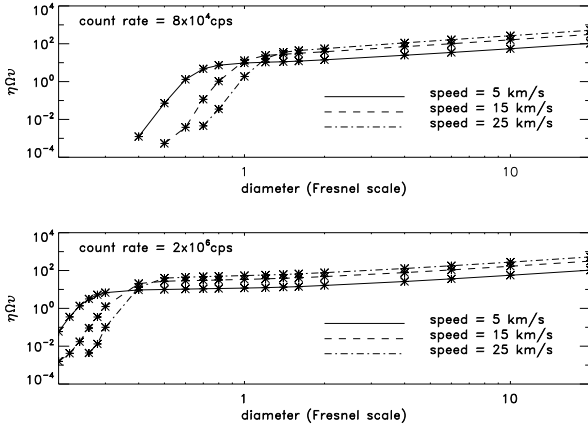


Figure 4. The product $\eta\Omega v$, in units of the Fresnel scale times km/s, as a function of the occulting body diameter. This product is a relative contribution to the event rate estimate from TNOs of different size and different transverse speeds.

For a background point source, the event rate can be estimated as (cf. Equation (8) in Chang et al. (2011))

$$\frac{N}{T} = \frac{\int_{D_1}^{D_2} \left(\frac{dn}{dD}\right) \eta\Omega v dD}{d^2} \times \left(\frac{180}{\pi}\right)^2, \quad (1)$$

where N is the number of detected events, T the total exposure time, $\left(\frac{dn}{dD}\right)$ the differential size distribution (in units of number per unit length per square degree), η the detection efficiency, Ω the shadow size, v the typical sky-projection relative speed, and d the typical distance to the TNOs. The product $\eta\Omega$ in the above equation was approximated by the diameter in Chang et al. (2011) The ratio of them as a function of occulting body diameter D is shown in Figure 3. The product $\eta\Omega v$ represents a certain relative detection probability. It is plotted in Figure 4 as a function of D for the three different speeds. We can see that the product $\eta\Omega v$ be-

comes one order smaller when the object diameter decreases from 20 Fresnel scale to 2 Fresnel scale. For the current RXTE/PCA count rate, it actually becomes relatively negligible for diameter smaller than 1 Fresnel scale. Nonetheless, $\frac{dn}{dD}$ as a function of D could be very steep, so the contribution to the event rate from objects of diameter between 1 and 2 Fresnel scale could be considerable. For the high count rate case, $\eta\Omega v$ becomes relatively negligible when the object diameter is smaller than 0.4 Fresnel scale.

We estimate the upper limit to the TNO size distribution at the level of setting $N = 1$ in Equation (1). Although different models in the literature give different predictions for the TNO size distribution of sizes smaller than about 100 km, a common trait among most models is a wavy shape, caused by the competition of coagulation, erosion and shattering in different size ranges, down to a small size of about 0.1 km (Kenyon & Bromley 2012), 0.5 km (Fraser 2009), or 1 km or so (Benavidez & Bagatin 2009), below which the collisional equilibrium is achieved. In the collisional equilibrium, one expects to have (O'Brien & Greenberg 2003) $\frac{dn}{dD} \sim D^{-q}$ and

$$q = \frac{7 + p/3}{2 + p/3}, \quad (2)$$

where p is the power index of the strength-size relation. In the so-called 'strength-scaled regime' (in contrast to the 'gravity-scaled regime' for larger bodies), p is negative. Most models give a q in the range from 3.5 to 4.0 for the collisional equilibrium. The distribution can be quite flat at the small-size end of the wavy-shape distribution. In Kenyon & Bromley (2012) q is about 1.0 in the range from 0.1 km to 1 km. If we describe the TNO size distribution in terms of

$$\frac{dn}{d \log D} = \left(\frac{dn}{d \log D}\right)_{D=D_0} \left(\frac{D}{D_0}\right)^{-q+1}, \quad (3)$$

we can have, from Equation (1),

$$\left(\frac{dn}{d \log D}\right)_{D=D_0} = \frac{1}{\int_{D_1}^{D_2} \left(\frac{D}{D_0}\right)^{-q+1} \frac{\eta\Omega}{D} dD} \frac{N}{T} \frac{d^2}{v} \left(\frac{\pi}{180}\right)^2 \ln 10, \quad (4)$$

where v is assumed to be a typical speed independent of D .

We consider two size ranges, that is, object diameter between 1.0 and 2.0 Fresnel scale and between 2.0 and 10.0 Fresnel scale. Assuming a typical distance $d = 40$ AU and a typical relative sky-projection speed $v = 25$ km/s, with $T = 334$ ks and setting one detection as the upper limit, we have in the size range from 30 m to 60 m (recall that one Fresnel scale is 30 m in the current case and whenever we use 'size' we mean the diameter) $\left(\frac{dn}{d \log D}\right)_{D=30 \text{ m}} < 4.0 \times 10^{11} \text{ deg}^{-2}$ for $q = 4.0$ and $\left(\frac{dn}{d \log D}\right)_{D=30 \text{ m}} < 3.3 \times 10^{11} \text{ deg}^{-2}$ for $q = 3.5$. In the size range from 60 m to 300 m we have $\left(\frac{dn}{d \log D}\right)_{D=60 \text{ m}} < 6.6 \times 10^{10} \text{ deg}^{-2}$ for $q = 4.0$, $\left(\frac{dn}{d \log D}\right)_{D=60 \text{ m}} < 5.7 \times 10^{10} \text{ deg}^{-2}$ for $q = 3.5$, and $\left(\frac{dn}{d \log D}\right)_{D=60 \text{ m}} < 1.2 \times 10^{10} \text{ deg}^{-2}$ for $q = 1.0$. Another factor of 1.14 should be applied to convert the estimate at the Sco X-1 latitude to the ecliptic; see the discussion right after Equation (11) in Chang et al. (2011) These upper limits are plotted in Figure 5.

Sources	Brightness (Crab)			λ	β	Other names
	4U	A1	ASMquick			
4U 1758-25	1.21	0.56	0.58	269.56	-1.63	1H1758-250, GX5-1
4U 1758-20	0.63	0.37	0.30	269.66	2.91	1H1758-205, GX9+1, Sgr X-3
4U 1617-15	17.95	9.1	11.0	245.14	5.73	1H1617-155, Sco X-1
4U 1813-14	1.00	0.33	0.37	273.24	9.35	1H1813-140, GX17+2, Ser X-2
4U 1702-36	0.79	0.41	0.44	258.11	-13.50	1H1702-363, GX 349+2, Sco X-2
4U 1642-45	0.48	0.18	0.25	255.31	-23.06	1H1642-455, GX340+0
4U 1837+04	0.30	0.14	0.12	280.60	28.09	1H1837+049, Ser X-1
4U 2142+38	0.58	0.47	0.38	345.98	47.96	1H2142+380, Cyg X-2
4U 1956+35	1.24	0.29	0.42	312.86	54.26	1H1956+350, Cyg X-1

Table 3. Non-extended bright X-ray sources, which are potential background targets for serendipitous TNO occultation search in X-rays. All the 9 listed sources are brighter than 0.1 Crab in all the 4th Uhuru (4U), HEAO 1 A-1 (A1), and RXTE All Sky Monitor (ASMquick) catalogues. The 4U catalog was compiled with observations conducted during 1972-1973, the A1 catalog was during 1977, and the ASMquick information is based on weekly average in August 2011. Those listed in the 2nd, 3rd and 4th columns are source brightness in the 4U, A1 and ASMquick catalogues respectively, all in units of a Crab. Their positions are in the 5th and 6th columns, where λ is the ecliptic longitude and β the ecliptic latitude, both in degrees. This list is sorted with the absolute value of the ecliptic latitude β .

4 SUMMARY AND DISCUSSION

We conclude the current effort of serendipitous TNO occultation search in X-rays with upper limits to the TNO size distribution in the size range from 30 m to 300 m. In RXTE/PCA observations of Sco X-1 from June 2007 to October 2011, only one non-instrumental dip event was found in the 334-ks data. Due to the distance-size degeneracy in the occultation light curve, one cannot easily determine the occulting body size or distance. One way to go around is to fit the light curve with different diffraction patterns and find the best-fit result of the relative transverse speed, which can be obtained only in units of Fresnel scale per unit time. Then with some orbital assumptions, this speed can be compared to the real relative transverse speed of a body at a certain distance to find the match (Chang et al. 2011). As discussed in Chang et al. (2011), based on the fitting result of the aforementioned approach, that non-instrumental dip event might be due to a TNO of 150-m size, but with a rare retrograde orbit, or, it might be due to an MBA of 40-m size, but the implied size distribution is incredibly steep, or, it might be due to a very nearby object of meter size moving at a relative speed of a few kilometers per second. The main reason of why there exists such a huge uncertainty in the result is the small number of photons detected at millisecond time scale.

Another possible way to break the distance-size degeneracy is to relax the assumption of the background star being a point source. The size of the X-ray emitting region in Sco X-1 is still under debate, ranging from about 50 km to 50,000 km, depending on different models. Sco X-1 is at a distance about 2.8 kpc. The corresponding angular size of its X-ray emitting region is 0.1 Fresnel scale at 40 AU considering the 50,000 km case. It is a good approximation to assume a point background source in such a case. On the other hand, if we are confident on the knowledge of the emitting region size and our instrument is large enough to provide good photon statistics, with a given angular size of the background source, one can detect the difference among diffraction shadow patterns caused by occulting bodies of the same size in units of Fresnel scale at different distances,

since the projection size of the background source at different distances are different in units of Fresnel scale. For Sco X-1, if the occulting body is in the inner Oort Cloud, say, at 4000 AU, its X-ray emitting region will appear to be 1-Fresnel scale large at that distance for the 50,000-km case. From detailed study of the occultation light curve, one may be able to distinguish the projection size of the background source in units of Fresnel scale and therefore to determine the distance. Again, this requires a larger instrument to provide good enough photon statistics.

After 16 years of fruitful service, RXTE was decommissioned in January 2012. Future projects of building larger instruments have been proposed, such as Athena (Barcons et al. 2012), AXTAR (Ray et al. 2011), and LOFT (Mignani et al. 2011). In particular, LOFT will be 20 times larger than RXTE/PCA in terms of its photon collecting power. In Table 3 and 4 we list 9 brightest non-extended X-ray sources suitable for serendipitous TNO occultation search in the LOFT era. X-ray sources tend to be variable. Those 9 sources are all brighter than 0.1 Crab in all the 4th Uhuru, HEAO 1 A1 and RXTE All Sky Monitor catalogues. See table captions for more details. Those 9 sources are located at different ecliptic latitude, providing the possibility to study latitude dependence of TNO distribution in the decimeter to hectometer size range. Their estimated LOFT count rates are also high enough to allow investigation in two or three energy bands, which can help to identify diffraction features and to determine whether the discovered dip events are occultation in nature. One of the 9 sources is a High-Mass X-ray Binary (HMXB) containing a black hole candidate. The other 8 are all Low-Mass X-ray Binaries (LMXBs), two of which are the so-called ‘Atoll sources’ and the other 6 are ‘Z sources’. They are all neutron-star systems showing various rich variation in their timing and spectral properties. Long-term monitoring of these 9 sources is by itself very much rewarding for the study of accretion physics around black holes and neutron stars, and is at the same time useful for pinning down the TNO size distribution in the decimeter and hectometer size range.

Sources	LOFT count rate			Brightness (Crab)	Type
	band (keV)	count rate (cps)	source fraction		
4U 1758-25	1-2	4.8×10^3	92.0%	1.02	Z source, Cyg X-2 like
	2-4	1.3×10^5	99.7%		
	4-6	1.2×10^5	99.7%		
	6-10	8.3×10^4	99.4%		
	10-20	2.1×10^4	95.4%		
4U 1758-20	1-2	1.3×10^4	97.0%	0.48	Atoll source
	2-4	6.6×10^4	99.5%		
	4-6	5.1×10^4	99.4%		
	6-10	4.1×10^4	98.8%		
	10-20	1.2×10^4	92%		
4U 1617-15	1-2	1.8×10^6	100%	12.6	Z source (Sco X-1)
	2-4	2.5×10^6	100%		
	4-6	1.1×10^6	100%		
	6-10	8.0×10^5	99.9%		
	10-20	2.4×10^5	99.6%		
4U 1813-14	1-2	6.9×10^3	94.4%	0.50	Z source, Sco X-1 like
	2-4	6.8×10^4	99.5%		
	4-6	5.6×10^4	99.4%		
	6-10	4.1×10^4	98.8%		
	10-20	1.4×10^4	93.1%		
4U 1702-36	1-2	1.8×10^4	97.8%	0.66	Z source, Sco X-1 like
	2-4	9.1×10^4	99.6%		
	4-6	7.1×10^4	99.6%		
	6-10	5.5×10^4	99.1%		
	10-20	1.7×10^4	94.3%		
4U 1642-45	1-2	1.3×10^3	69.1%	0.34	Z source, Cyg X-2 like
	2-4	3.8×10^4	99.1%		
	4-6	4.4×10^4	99.3%		
	6-10	3.0×10^4	98.3%		
	10-20	7.3×10^3	86.8%		
4U 1837+04	1-2	1.8×10^4	97.9%	0.21	Atoll source
	2-4	3.3×10^4	98.9%		
	4-6	2.0×10^4	98.4%		
	6-10	1.7×10^4	97.1%		
	10-20	7.1×10^3	86.4%		
4U 2142+38	1-2	1.7×10^4	97.8%	0.44	Z source (Cyg X-2)
	2-4	7.6×10^4	99.5%		
	4-6	4.6×10^4	99.3%		
	6-10	3.0×10^4	98.4%		
	10-20	8.6×10^3	88.8%		
4U 1956+35	1-2	4.6×10^4	99.1%	0.5	black hole candidate, HMXB
	2-4	7.3×10^4	99.5%		
	4-6	4.5×10^4	99.3%		
	6-10	4.4×10^4	98.9%		
	10-20	3.0×10^4	96.8%		

Table 4. Estimated LOFT count rates for the 9 sources listed in Table 1. These count rates are estimated with LOFT response files and are based on spectral models reported in the literature (4U 1758-25: Jackson, Church & Balucinska-Church (2009); 4U 1758-20: Iaria et al. (2005); 4U 1617-15: Bradshaw, Geldzahler & Fomalont (2003); 4U 2142+38: Balucinska-Church et al. (2010); 4U 1956+35: Nowak et al. (2011); the other 4 sources: Cackett et al. (2009)). Those listed count rates are the total count rate (including background). The brightness, in units of a Crab, in the 5th column is based on the assumed spectral model and is for the 2-10 keV band, in which a Crab is 2.4×10^{-8} erg cm $^{-2}$ sec $^{-1}$.

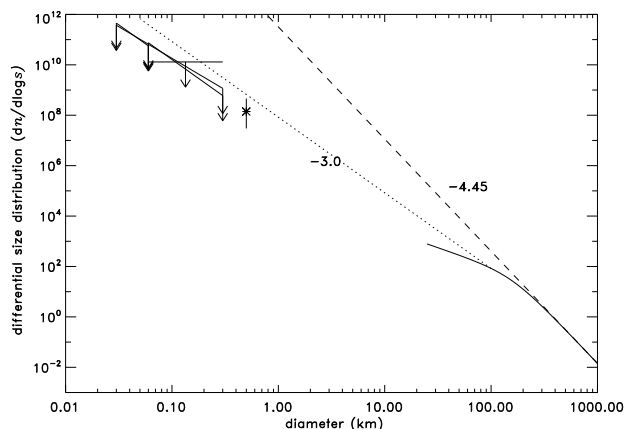


Figure 5. The TNO size distribution. Plotted here is the differential sky surface density at the ecliptic per decade of size in units of number per square degree. The upper limits in the size range of 30-60 m and of 60-300 m, denoted with downward arrows, are derived from our non-detection in the 334-ks RXTE/PCA data of Sco X-1, and is set at the level of one detection in 334 ks. The cases of q equal to 3.5 and 4.0 ($\frac{dn}{d \log D} \sim D^{-q+1}$) are considered in the two size ranges, of which the derived upper limits are very close to each other as plotted in this figure. The case of q equal to 1.0 is also considered in the size range of 60-300 m. The downward arrows are plotted at the size-range boundary for q equal to 3.5 and 4.0, and at the middle of the size range for q equal to 1.0. The asterisk symbol at 0.5 km is based on the reported HST/FGS detection of an occultation event (Schlichting et al. (2009); see also Schlichting et al. (2012)). The solid curve is the double-power-law distribution of large TNOs (Fuentes et al. 2010); see Chang et al. (2011) for the assumptions made to convert the luminosity function to the size distribution. The dashed line is a direct extrapolation from the large size end of the double-power-law towards smaller size and the dotted line is a power law anchoring on the double-power-law at 90 km with a power index of -3.0. We note that the power indices in this figure, explicitly printed close to the corresponding power-law lines, are for the differential size distribution per decade of size, and are therefore the same as that of the cumulative size distribution. The double-power-law and the HST/FGS result in fact indicate a wavy shape for the TNO size distribution, similar to that of the main-belt asteroids.

ACKNOWLEDGMENTS

We thank Ed Morgan, who designed the new RXTE/PCA data mode and coordinated the new RXTE observations of Sco X-1. This work was supported by the National Science Council of the Republic of China under grants NSC 99-2112-M-007 -017 -MY3 and 101-2923-M-007 -001 -MY3.

REFERENCES

Barcons X. et al., 2012, arXiv:1207.2745
 Benavidez P. G., Bagatin A. C., Planetary and Space Science, 57, 201
 Bianco F.B. et al., 2010, AJ, 139, 1499
 Bickerton S.J., Kavelaars J.J., Welch D.L., 2008, AJ, 135, 1039
 Bradshaw C. F., Geldzahler B. J., Fomalont E. B., 2003, ApJ, 592, 486
 Cackett E. M. et al., 2009, ApJ, 690, 1847

Chang H.-K., King S.-K., Liang J.-S., Wu P.-S., Lin L.C.-C., Chiu J.-L., 2006, Nature, 442, 660
 Chang H.-K., Liang J.-S., Liu C.-Y., King S.-K., 2007, MNRAS, 378, 1287
 Chang H.-K., Liu C.-Y., Chen K.-T., 2011, MNRAS, 411, 427
 Chiang E., Lithwick Y., Murray-Clay R., Buie M., Grundy W., Holman M., 2007, in Protostars and Planets V, B. Reipurth, D. Jewitt, and K. Keil (eds.), University of Arizona Press, Tucson, p.895-911
 Balucinska-Church M., Gibiec A., Jackson N. K., Church M. J., 2010, A&A, 512, A9
 Fraser W. C., 2009, ApJ, 706, 119
 Fraser W. C., Brown M. E., Schwamb M. E., 2010, Icarus, 210, 944
 Fuentes C. I., Holman M. J., Trilling D. E., Protopapas P., 2010, ApJ, 722, 1290
 Fuentes C. I., Trilling D. E., Holman M. J., 2011, ApJ, 742:118
 Iaria R., Di Salvo T., Robba N. R., Lavagetto G., Burderi L., Stella L., van der Klis M., 2005, A&A, 439, 575
 Jackson N. K., Church M. J., Balucinska-Church M., 2009, A&A, 494, 1059
 Jahoda K. et al., 2006, ApJS, 163, 401
 Jones T.A., Levine A.M., Morgan E.H., Rappaport S., 2008, ApJ, 677, 1241
 Kenyon S. J., Bromley B. C., 2012, AJ, 143:63
 Liu C.-Y., Chang H.-K., Liang J.-S., King S.-K., 2008, MNRAS, 388, L44
 Mignani R. P. et al., 2011, in Proceedings of the IAU, 7, pp 372-375
 Nihei T.C., Lehner M.J., Bianco F.B., King S.-K., Giannamarco J.M., Alcock C., 2007, AJ, 134, 1596
 Nowak M. A. et al., 2011, ApJ, 728:13
 O'Brien D.P., Greenberg R., 2003, Icarus, 164, 334
 Petit J.-M. et al., 2011, AJ, 142:131
 Ray P. S., Philips B. F., Wood K. S., Chakrabarty D., Remillard R. A., Wilson-Hodge C. A., 2011, arXiv:1109.1309
 Roques F. et al., 2006, AJ, 132, 819
 Roques F., Moncuquet M., Lavilloniere N., Auvergne M., Chevreton M., Colas F., Lecacheux J., 2003, ApJ, 594, L63
 Roques F., Moncuquet M., Sicardy B., 1987, AJ, 93, 1549
 Schlichting H.E., Ofek E.O., Wenz M., Sari R., Gal-Yam A., Livio M., Nelan E., Zucker S., 2009, Nature, 462, 895
 Schlichting H.E., Ofek E.O., Sari R., Nelan E., Gal-Yam A., Wenz M., Muirhead P., Javanfar N., Livio M., 2012, arXiv:1210.8155